Computers and Geotechnics 161 (2023) 105559

Contents lists available at ScienceDirect

Computers and Geotechnics

journal homepage: www.elsevier.com/locate/compgeo

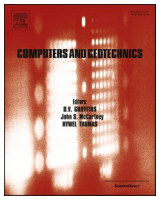

DEM study of particle scale effect on plain and rotary jacked pile behaviour in granular materials

B. Cerfontaine [a,*], M.O. Ciantia [b], M.J. Brown [b], D.J. White [a], Y.U. Sharif [b]

[a] Engineering and Physical Sciences, University of Southampton, Boldrewood campus, Southampton, UK
[b] School of Science and Engineering, University of Dundee, Fulton Building, Dundee DD1 4HN, UK

ARTICLE INFO

Keywords:
Discrete Element Method
Rotary jacking
Pile jacking
Plugging

ABSTRACT

The capacity of open-ended piles strongly depends on the potential plugging occurring during installation. The Discrete Element Method (DEM) is particularly suitable to the study of pile plugging, as it can model large soil deformation. However, DEM simulation of the 3D boundary value problems is computationally expensive, and particle upscaling is usually used to reduce the number of particles modelled. In this paper, two granular beds were created with the same average porosity, initial stress field and contact parameters, but different particle scales. Two pile geometries were installed by plain and rotary jacking. Normalised results show that the pile penetration mechanism is strongly affected by the particle scale. Larger particles lead to earlier pile plugging, higher shaft resistance and require a greater force to penetrate the ground. This effect can be linked to a modified penetration mechanism, with larger shear zones and less well defined "nose cone" under the pile tip for larger particles. Changing particle scaling has a neutral effect on the total penetration resistance of a rotary jacked pile, but reduces the base penetration and increases the plug resistance. Maximising the ratio of particle scale to wall thickness is key to adequately capturing the pile coring mechanism.

1. Introduction

Plain (i.e. vertical) jacking or rotary pile jacking can be a silent alternative to pile driving in urban environments (Deeks et al., 2010; Ishihara et al., 2020) or offshore (Cerfontaine et al., 2021a) where noise and vibrations emissions are increasingly restricted. Large tubular piles, such as those used offshore, are usually open-ended and prone to pile plugging when jacked into the ground, which affects their axial capacity (Paikowsky and Whitman, 1990; Deeks et al., 2010). Pile plugging confers a greater capacity to jacked piles than to driven piles, but a large reaction force is needed to install them. The use of rotary jacked piles, in which the piles are pushed vertically while also rotated about the vertical axis, significantly reduces this need for additional reaction force during installation (Deeks et al., 2010; Brown and Ishihara, 2021; Sharif et al., 2021c), at the expense of a pile capacity reduction. In all cases, the ultimate pile capacity depends on the installation process and any associated plugging (Jardine et al., 2005; Lehane et al., 2007), which should be accurately predicted to design reliable and cost-effective piles. Field tests are often used to study pile plugging, for instance by using highly instrumented double-wall piles (Suits et al., 2010, 2011; Han et al., 2020), which provides useful information such as local stress, strain or pore water pressure measurements. While field tests are generally used to demonstrate the feasibility of new technologies, they remain expensive and subject to soil variability. Therefore, other methods can be used to complement field testing, especially at the early stages of technology development when several concepts must be investigated or where physical mechanisms need be identified.

The Discrete Element Method (DEM) has been widely used to investigate fundamental soil behaviour at the element scale (Khoubani and Evans, 2018; Shire et al., 2020). More recently, this method has been used to uncover relevant micromechanical mechanisms involved in boundary value problems such as cone penetration resistance (Zhang and Wang, 2015; Ciantia et al., 2016) or pile penetration (Esposito et al., 2018; Ciantia et al., 2019; Li et al., 2021). Recent studies have shown that the DEM can successfully predict the behaviour of small-scale models representative of large scale offshore foundations tested in a geotechnical beam centrifuge (Cerfontaine et al., 2021b; Sharif et al., 2021a) or calibration chamber (Ciantia et al., 2019). Sharif et al., (2021c) and Zhang and Fatahi (2021) also showed that DEM simulations can identify contributions from base or shaft of the pile, as well as calculation of stress distribution along the shaft giving greater insights

* Corresponding author.
E-mail addresses: b.cerfontaine@soton.ac.uk (B. Cerfontaine), m.o.ciantia@dundee.ac.uk (M.O. Ciantia), m.j.z.brown@dundee.ac.uk (M.J. Brown), david.white@soton.ac.uk (D.J. White), y.u.sharif@dundee.ac.uk (Y.U. Sharif).

https://doi.org/10.1016/j.compgeo.2023.105559
Received 2 December 2022; Received in revised form 22 May 2023; Accepted 23 May 2023
Available online 6 June 2023

Nomenclature

Notation

D	Pile diameter
d_{50}	Median particle dimension
F_b	Resultant force acting on the annular base
$F_{s,i}$	Resultant vertical force acting on the inside of the pile shaft
$F_{s,o}$	Resultant vertical force acting on the outside of the pile shaft
F_{tot}	Total vertical force acting on the pile
F_z	Component of the contact force acting in the vertical direction
F_θ	Component of the contact force acting in the orthoradial direction
F_ρ	Component of the contact force acting in the radial direction
IFR	Incremental Filling Ratio
L_{plug}	Length of the plug
N	Model scaling factor
P1, P2	Pile P1 (0.5 m diameter) or P2 (0.7 m diameter)
p_i	Installation pitch
R_a	Pile radius
SF	Particle scaling factor
u_z	Local vertical direction
u_ρ	Local radial direction
u_θ	Local orthoradial direction
t	Pile wall thickness
v_z	Vertical instantaneous velocity of the pile during installation
X, Y, Z	Absolute coordinates
z	Tip depth
ρ	Radial distance
$\sigma_{n,b}$	Normal stress acting on the annular base
$\sigma_{n,p}$	Normal stress acting on the plug base
$\sigma_{\rho,i}$	Radial stress acting on the inside of the pile
$\sigma_{\rho,o}$	Radial stress acting on the outside of the pile
$\tau_{v,o}$	Vertical shear stress acting on the outside of the pile
ω	Pile rotation rate during installation

into installation effects.

Most DEM studies devoted to pile plugging or pile installation are limited to 2D simulations (Lobo-Guerrero and Vallejo, 2007; Liu et al., 2019; Duan et al., 2021; Li et al., 2021) to limit the computational cost. Some authors adopted a 2.5D approach, for instance by using an angular fraction of a calibration chamber (McDowell et al., 2012; Zhang and Fatahi, 2021). However, modelling of plugging and especially rotary jacking require 3D DEM simulations, which are very computationally expensive. Particle upscaling, where dimensions of simulated particles are larger than their real size is commonly used to reduce this computational cost (Arroyo et al., 2011). However, if particles are too large with respect to the pile, the soil-structure interactions during installation can be modified.

Previous DEM studies have shown that tool or plate penetration resistance increases with a decrease in the ratio of plate thickness to median particle dimension. (Lommen et al., 2019; Miyai et al., 2019). Miyai et al., 2019 recommend, based on 2D simulations, that this ratio should be greater than 30 to avoid particle scale effects. Similar issues arise for centrifuge geotechnical modelling of CPT and pile installation. It has been shown that a ratio of CPT diameter to grain size of > 20 is recommended to eliminate scale effects (Bolton et al., 1999). However, for open-ended piles, published studies has used ratios of pile wall thickness to median particle diameter ratios ranging from 2.7 to 17 with minimal scaling effects (Henke and Bienen, 2014; Bienen et al., 2018; Fan et al., 2019). Particle scale effects also occur in field studies and design. It was shown that the measured resistance, and particularly the shaft resistance, of open-ended piles driven in gravel or gravelly sand was significantly lower than predicted by well-established CPT-based methods developed in (Jeanjean et al., 2015; Han et al., 2020). The pile wall thickness to particle dimension ratio ranged between 0.5 and 2.0 in those studies.

Firstly, the goal of this paper is to explore pile penetration mechanisms and identify particle scale effects during simulation of plain and rotary jacking of open-ended piles. Secondly, this work aims to explore solutions and provide guidance to make the DEM a more reliable and less computationally intensive prediction method for boundary value problems such as pile installation. 3D DEM simulations of two pile geometries were undertaken in two granular beds, using varying particle sizes and a truncated servo-controlled soil domain to limit the computational cost of the simulations. The results combine macroscopic (e.g. forces, base stress) with "microscopic" (particle displacement, force chains) results, to identify relevant physical mechanisms during installation and understand how they are affected by the particle sizes. Recommendations for DEM simulations are provided based on the various observations.

2. Methodology

2.1. Calibration chamber

The DEM, with PFC3D 6.00.17 (Itasca Consulting Group, 2019), was used to create a virtual centrifuge environment with an enhanced gravity (model scaling factor $N = 50$) to mimic the conditions of centrifuge tests (Ciantia et al., 2018). This calibration chamber was described in detail in Cerfontaine et al. (2021b) and only the most important features are described herein.

Two polydisperse granular beds were created based on a particle size distribution and parameters representative of the HST95 sand (Table 1) and determined by standard laboratory test. The beds used upscaled particle sizes (with respect to the real sand particles) using scaling factors (SF) equal to 10 and 20. The upscaled particles have the size of gravel and boulders. The target average void ratio of each sample was equal to 0.61 (equivalent to 52% relative density for HST95) and the stress state corresponded to a coefficient of earth pressure at rest of $K_0 = 0.47$. By following the procedure described in Ciantia et al., (2018), which consists of stacking smaller representative elementary volumes

Table 1
HST95 sand physical properties after (Lauder, 2010; Al-Defae et al., 2013) and contact model properties after (Sharif et al., 2019).

Physical properties [unit]			
Minimum void ratio [-]	e_{min}	0.467	
Maximum void ratio [-]	e_{max}	0.769	
Critical state friction angle [°]	ϕ_{cs}	32	
Sand-steel interface friction angle [°]	δ	24	
Particle diameter (10% mass passing) [mm]	d_{10}	0.09	
Median particle diameter [mm]	d_{50}	0.141	
Maximum particle diameter [mm]	d_{100}	0.213	
Particle density [kg/m^3]	ρ_s	2650	
DEM parameters [unit]			
Particle shear modulus [GPa]	G		3
Particle Poison's ratio [-]	ν		0.3
Particle friction coefficient [-]	μ		0.264
Pile interface friction coefficient [-]	μ_{pile}		0.445
Wall interface friction coefficient [-]	μ_{wall}		0.8

(REV) (seven in this case) to create a final granular bed, the time required to create the initial conditions was of 12 and 36 hrs of simulation time SF equal to 10 and 20 respectively (computers specifications: Intel® Xeon® CPU E5-1650 v4 @3.60 GHz, 48 GB RAM, 64-bit operating system).

The cylindrical calibration chamber was 10.5 m high and its diameter was equal to 4.25 m. The distance from the pile centreline to the boundary was equal to at least 3 pile diameters. The potential boundary effect due to the short distance between the pile and the boundary was minimised by seven radially servo-controlled cylinders (one per initial REV, see Fig. 1a-b), which imposed a constant elastic radial stiffness along the boundary, corresponding to the secant shear modulus of HST95 sand, as calibrated for the hardening soil model (Al-Defae et al., 2013). The formulation of the servo-control assumes that the mean and vertical stresses remain constant at the boundary. The pile-wall friction coefficient was set up to 0.8, which corresponds to the HST95 sand peak friction angle at the same porosity, to simulate a rough interface and to reduce potential particle movement due to the shear stress induced by rotary jacking. Such a calibration chamber reduces the necessary number of particles, hence the computational time, required to undertake simulations with the smallest SF.

2.2. Pile model

Two pile models P1 and P2 were considered in this study (see Fig. 1c), with external diameters (D) equal to 0.5 m and 0.7 m respectively at prototype scale. The shaft (D) to median particle (d_{50}) diameter ratio ranges between 3.5 and 10 (see Table 2), which is in the range of published studies (2 to 6 for 3D simulations) as described by Ciantia et al. (2019). The pile wall thickness (t) was identical in both cases and equal to 0.02 m, and the resulting ratio t/d_{50} is equal to 0.28 and 0.14 for particle size scale factors (SF) of 10 and 20 respectively. This ratio is lower than those recommended for centrifuge modelling (see section 1), but the use of smaller particles was not computationally affordable in 3D.

The pile was modelled as rigid, and it was installed by specifying rotation (ω) and vertical displacement (v_z) rates along its axis. The installation pitch (p_i) is defined as

Table 2
Estimation of the large deformation friction coefficient based on the relationship proposed by Ho et al. (2011). The median particle dimension is the one of the HST95 sand and the pile roughness is taken equal to 5 or 10 μm.

Scaling factor, SF	*1*		*10*		*20*	
Actual median diameter, d_{50} [mm]	*0.141*		*1.41*		*2.82*	
Pile steel roughness, R_a [μm]	*10*	*5*	*10*	*5*	*10*	*5*
Normalised roughness, $\frac{R_a}{d_{50}} \times 1000$	*71.0*	*35.5*	*7.1*	*3.55*	*3.5*	*1.75*
Estimated friction coefficient, μ [-]	*0.553*	*0.499*	*0.456*	*0.450*	*0.450*	*0.448*

$$p_i = \frac{\omega D}{2 v_z} \tag{1}$$

The pitch is equal to zero for plain jacking, and was set to 1.73 and 10 for rotary jacking cases, as was previously used by Sharif et al., (2021c). This range is consistent with typical values used in practice, for instance 3.5 for the Gyropiler (Deeks et al., 2010).

2.3. Contact model

The contact model used in this study was a modified Hertz-Mindlin relationship which is described in detail in the documentation of Itasca Consulting Group (2019). A single set of DEM particle parameters (Table 1) was calibrated independently against triaxial tests by Sharif et al. (2019), irrespective of the SF, as normal stiffness is calculated automatically as a function of particle size (Lommen et al., 2019). The parameters are broadly consistent with parameters identified for other sand materials (Huang et al., 2014; Ciantia et al., 2019; Wu et al., 2022). The pile-particle interface friction coefficient ($\mu_{pile} = 0.445$) was determined by direct sand-steel shear tests (Lauder et al., 2013). The actual large deformation friction coefficient depends on the pile roughness and particle size, and can be estimated by a relationship proposed by Ho et al. (2011). The friction coefficients calculated for each SF and a pile roughness ranging from 5 to 10 μm (Jardine et al., 2005) are given in Table 2. The friction coefficient adopted in the simulations ($\mu_{pile} = 0.445$) is lower that what would be expected for real scale particles (SF

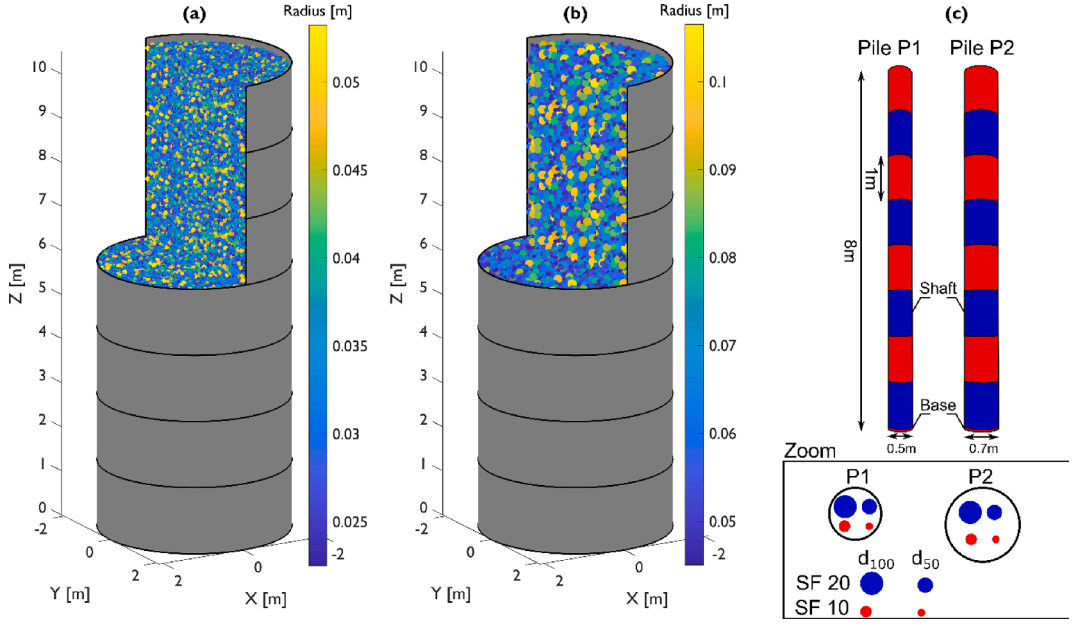

Fig. 1. (a-b) Half soil beds and servo-controlled cylinders for SF = 10 and 20 respectively. (c) Open-ended pile models (P1 & P2) and comparison of their cross-section with the particle size shown in the zoomed-in zone.

$= 1$, $\mu_{pile} \geq 0.5$), but is consistent with the size of particles adopted in the simulations (SF = 10 or 20, $\mu_{pile} \approx 0.45$). It should also be noted that the pile surface is geometrically perfectly smooth, even if it is given frictional properties. This smoothness can affect the overall interface behaviour by reducing the potential dilative behaviour due to the actual steel roughness, as shown by Martinez and Frost (2017).

Particle rotation was inhibited to roughly simulate the interlocking effects due to non-spherical particle shapes. This is a computationally efficient simplification (Ting et al., 1989; Calvetti, 2008; Arroyo et al., 2011) that may be seen as a limit case for classical rolling-resistance contact models (Rorato et al., 2021).

2.4. Summary of simulations

The vertical displacement and rotation rates were applied to the piles to simulate continuous jacking at a constant installation pitch (p_i). These rates were calculated to ensure quasi-static conditions, following a procedure detailed in previous studies (Ciantia et al., 2019; Cerfontaine et al., 2021b; Sharif et al., 2021b). Seven simulations (Table 3) were undertaken for a total of more than 43 days of simulations. The effect of the SF for plain jacking was investigated for the two pile diameters (ID 1 to 4) in the two granular beds (SF = 10 and 20). Then this effect was tested for rotary jacking of pile P2.

3. Results and discussion

The effects of the particle SF on axially jacked piles are evaluated first, as these results can be qualitatively compared with the existing literature. Macroscopic and microscopic observations are used to identify and discuss the physical mechanisms occurring during installation and how they are affected by particle scaling. Results of rotary jacked piles are analysed similarly afterwards.

3.1. Effect of SF on plain jacking

3.1.1. Macroscopic observations

For each simulation, the vertical forces acting on the pile annular base (F_b), the inside ($F_{s,i}$) and the outside ($F_{s,o}$) of the shaft were measured independently. The plug length, L_{plug}, was measured as the distance between the highest particle inside the pile and the tip. The incremental filling ratio is the rate at which the plug length is increasing (dL_{plug}) with pile penetration (dz), and is defined as IFR = dL_{plug}/dz. Results were scaled up from model to prototype scale (velocity 1:1, distance 1:N and force $1:N^2$, with N = 50) according to centrifuge scaling laws (Garnier et al., 2007).

Fig. 2 compares the behaviour of the two piles (P1 and P2) in the two granular beds (SF = 10 or 20) and numerical values at the end of installation are given in Table 4. Table 4 shows that the total penetration resistance (F_{tot}) is increased by 48% and 36% for P1 and P2 respectively, when the SF is increased from 10 to 20. This increase is mainly due to a rise in base force (F_b in Fig. 2a-b), which represents 50–65% of the total force at z = 8 m. Conversely, the pile internal resistance decreases for P2 only, when SF is increased (Fig. 2b). Finally, Fig. 2c shows that, at a given depth, smaller particles and bigger piles experience a greater IFR. This figure shows that the piles are partially plugged for most of the simulation and are almost fully plugged (IFR≈0) at the end, with only P2 experiencing true coring at the beginning.

Table 3
Summary of the simulations undertaken, particle scaling factor (SF), pile diameter (D), pile diameter to median particle diameter ratio (D/d_{50}), pile wall to median particle diameter ratio (t/d_{50}), installation pitch (p_i) and installation simulation duration.

ID	SF [-]	Pile	D/d_{50} [-]	t/d_{50} [-]	p_i [-]	Duration [d]
1	10	P1 (D = 0.5 m)	7.1	0.28	0	11.1
2	20		3.5	0.14	0	1.8
3	10	P2 (D = 0.7 m)	10.0	0.28	0	11.5
4	20		5.0	0.14	0	2.0
5	20		5.0	0.14	1.73	1.9
6	10		10.0	0.28	10	12.2
7	20		5.0	0.14	10	2.0

Fig. 3 shows normalised results to account for different pile diameters and identical pile wall thicknesses. The normal stress acting on the pile annular base ($\sigma_{n,b}$) was calculated by using F_b, while the internal shaft resistance ($F_{s,i}$) was used as a proxy to calculate the normal stress acting on the plug base ($\sigma_{n,p}$),

$$\sigma_{n,p} = \frac{4F_{s,i}}{\pi D_i^2} \tag{2}$$

where D_i is the internal shaft diameter and the weight of the plug was neglected.

The normal stress acting on the annular base ($\sigma_{n,b}$ in Fig. 3a) is initially identical for a given SF (grey or black curves in Fig. 3a), despite different pile diameters. Then the normal stress diverges beyond a certain depth (e.g. 2.6 m for SF = 20, grey curves). The same phenomenon is observed for the plug base stress ($\sigma_{n,p}$ in Fig. 3b). This is consistent with the two modes of penetration of the pile: coring and plugging.

When coring takes place (IFR → 1), the internal shaft resistance ($F_{s,i}$) is insufficient to oppose the flow of soil inside the pile. The stress acting on the annular base ($\sigma_{n,b}$) is independent of the pile diameter. The soil failure mechanism is local, with the soil flowing on both sides of the pile wall (see section 3.1.2), similarly to plane strain conditions. Scaling effects are related to the t/d_{50} ratio, which shows that larger particles lead to greater penetration resistance, as shown by Lommen et al. (2019) and Miyai et al. (2019), hence the clustering of results as a function of SF, i.e. black curves close to each other.

When significant plugging starts to take place (IFR → 0), the dimensionless plug length ($= L_{plug}/D$) growth slows down (Fig. 3d). It becomes more difficult for particles to enter the pile, and this particle jamming leads to some base stress build up ($\sigma_{n,p}$, in Fig. 3b). The failure mechanism approaches the one of a closed-ended pile, i.e. particles flow around the pile (Li et al., 2020). The base and plug stresses start diverging for different pile diameters (Fig. 3a,b) at the same SF, which suggests that scaling effects in this case depend on the D/d_{50} ratio.

From Fig. 3a,b, it can be observed that the stress acting on the annular base ($\sigma_{n,b}$) is much higher than the one acting on the plug base ($\sigma_{n,i}$), even when behaviour tends to full plugging (IFR → 0). This contrasts to conventional plugging analysis, which assumes these are equal, when a plug forms (Paikowsky and Whitman, 1990). This evolution of the base to plug stress ratio ($\sigma_{n,b}/\sigma_{n,p}$) as a function of the IFR, is further used as a proxy to identify penetration mechanism (from coring to plugging) and shows clear scaling effects (Fig. 4). The plug becomes stable when the ratio reaches a value ranging between 12 and 40 for SF equal to 10 or 20 respectively. These values of $\sigma_{n,b}/\sigma_{n,p}$ can be compared with other numerical or experimental results. Li et al., (2020) calculated ratio values ranging from 2 and 3.2 in plane strain DEM modelling of open-ended piles ($R/t = 3.5 - 13.5$). Igoe *et al.*, (2010) measured a ratio of about 4 ($R/t = 9.5$) with instrumented piles installed in sand.

Finally, Fig. 3c shows the average shear stress ($\tau_{v,o}$) distribution along the outside shaft. Results are clustered by SF, with larger shear stress associated with larger SF. Results for SF = 20 (grey curves in Fig. 3c) also diverge, which is probably linked to the pile plugging behaviour. Earlier pile plugging creates more soil lateral displacement and will enhance the radial stress acting on the shaft outside wall, as described by White et al. (2005).

Based on previous observations, it can be concluded that granular beds with SF = 10 and 20 behave as distinct soils, within the range of simulated conditions, despite their assigned properties being identical. This is particularly clear for the annular base stress or outer shaft

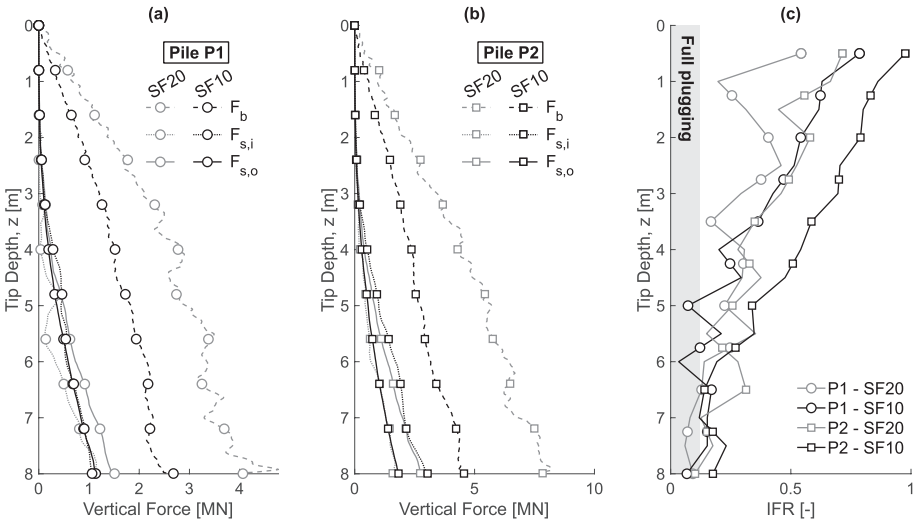

Fig. 2. Base (F_b), internal shaft ($F_{s,i}$) and external ($F_{s,o}$)vertical forces acting on piles (a) pile P1 (D = 0.5 m) and (b) pile P2 (D = 0.7 m) during the plain jacking installation, (c) Incremental filling ratio (IFR).

Table 4
Measured components of force at the end of the installation for plain jacking.

Pile	SF	F_{tot} [MN]	F_b [MN]	$F_{s,i}$ [MN]	$F_{s,o}$ [MN]
P1	10	4.4	2.4	1.0	1.1
	20	6.6	4.1	1.1	1.4
	10 → 20	+48%	+75%	+7%	+28%
P2	10	8.8	4.4	2.8	1.7
	20	12.0	7.8	1.6	2.6
	10 → 20	+36%	+79%	−42%	+52%

mobilised shear strength. Comparison of the annular base stress ratio with field tests or 2D DEM simulations also showed that the SF = 10 granular bed is probably also affected by scaling issues, although their magnitude is lower with respect to SF = 20. However, scaling issues are related to a specific failure mechanism, in this case coring, and to a representative geometrical ratio, in this case t/d_{50}. Indeed, it has been shown in previous studies that satisfactory results can be obtained for closed-ended piles or probe penetration in granular beds for which the representative geometrical ratio, D/d_{50} ranges from 2.7 to 5.8 (Arroyo et al., 2011; Zhang and Wang, 2015; Khosravi et al., 2020). The D/d_{50} ratio ranges from 3.5 to 10 in this work.

3.1.2. Microscopic observations

In the previous section, the evolution of the measured forces were correlated to the plugging behaviour of the pile, via the IFR. However, the DEM offers the opportunity to actually observe the pile plugging, particle displacement and the development of contact forces around the pile.

Fig. 5a depicts a cross-section of the particles at the end of plain jacking of pile P2 (SF = 10). Particles are coloured as a function of their initial position in a layered manner. Fig. 5a shows high shearing along the shaft, outside of the pile and in the upper part of the plug. Fig. 5a also shows that the soil below the pile tip is deflected (in the nose cone) and the lowermost layers of the pile plug are thinner as a consequence. Force chains depicted in Fig. 5c show large magnitude forces just under the tip and inside the pile plug. The largest magnitude forces initiate just under the annular base, and some of these propagate to the outer boundary.

These results are consistent with DEM results of Li et al. (2019, 2020) and the interpretation is summarised in Fig. 6a-b. At shallow depth, the pile is coring (Fig. 6a). The particles flow around pile walls, and the centre of the pile plug is only slightly affected. Load transfer from the

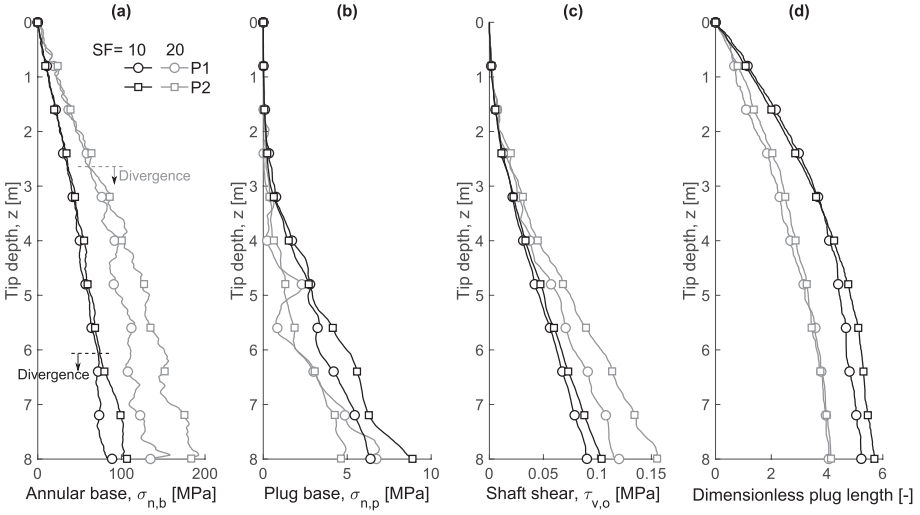

Fig. 3. Normalised results: (a) Normal stress on the pile annular base ($\sigma_{n,b}$); (b) Normal stress on the plug base ($\sigma_{n,p}$); (c) Average shear stress on the external part of the shaft ($\tau_{v,o}$); (d) Dimensionless plug length (L_{plug}/D).

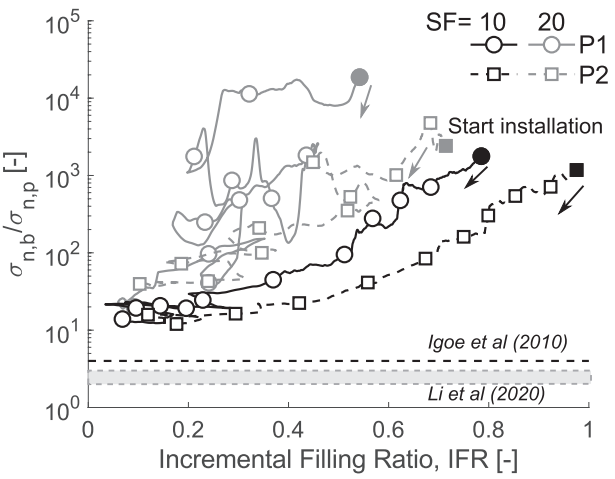

Fig. 4. Ratio of the stress acting on the annular base to the average plug stress as a function of the incremental filling ratio (IFR). The state at the beginning of the simulation is denoted by a coloured marker.

pile shaft only occurs in a localised shear zone nearby the walls and under the tip.

As the pile penetration continues, the load transfer mechanism creates larger shear zones, which start to interact with each other inside the pile, and plugging takes place eventually (Fig. 6b). Shearing is reduced inside the plug and a granular "nose cone" forms under the tip (White and Bolton, 2004; Li et al., 2020). This cone deflects the soil under the tip and creates a flow of particles around the pile, while shearing continues outside the shaft. Arching takes place within this zone, hence the large force chains in the area.

The ability of the DEM to quantitatively predict the pile penetration resistance depends on the possibility to simulate shear zones and slip surfaces, whose thickness is typically in the range of 5 to 30d_{50} (Desrues and Viggiani, 2004). Fig. 5b, depicts particles at the end of installation for SF = 20 and shows that the width of shear zones outside of the pile, along the shaft, is approximately twice the one measured for SF = 10 (Fig. 5a). The shear band close to the pile tip (in Fig. 5a,b) width can be roughly estimated to be 0.17 m and 0.4 m large for SF = 10 and = 20 respectively. It can be assumed that shear bands inside the pile were also wider and started to interact at a shallower depth, hence the earlier plugging for larger SF.

The highly concentrated force chains identified in Fig. 5 and high base stresses shown in Fig. 3 suggest that some particles are exposed to very large concentration of forces. In reality, particle crushing may

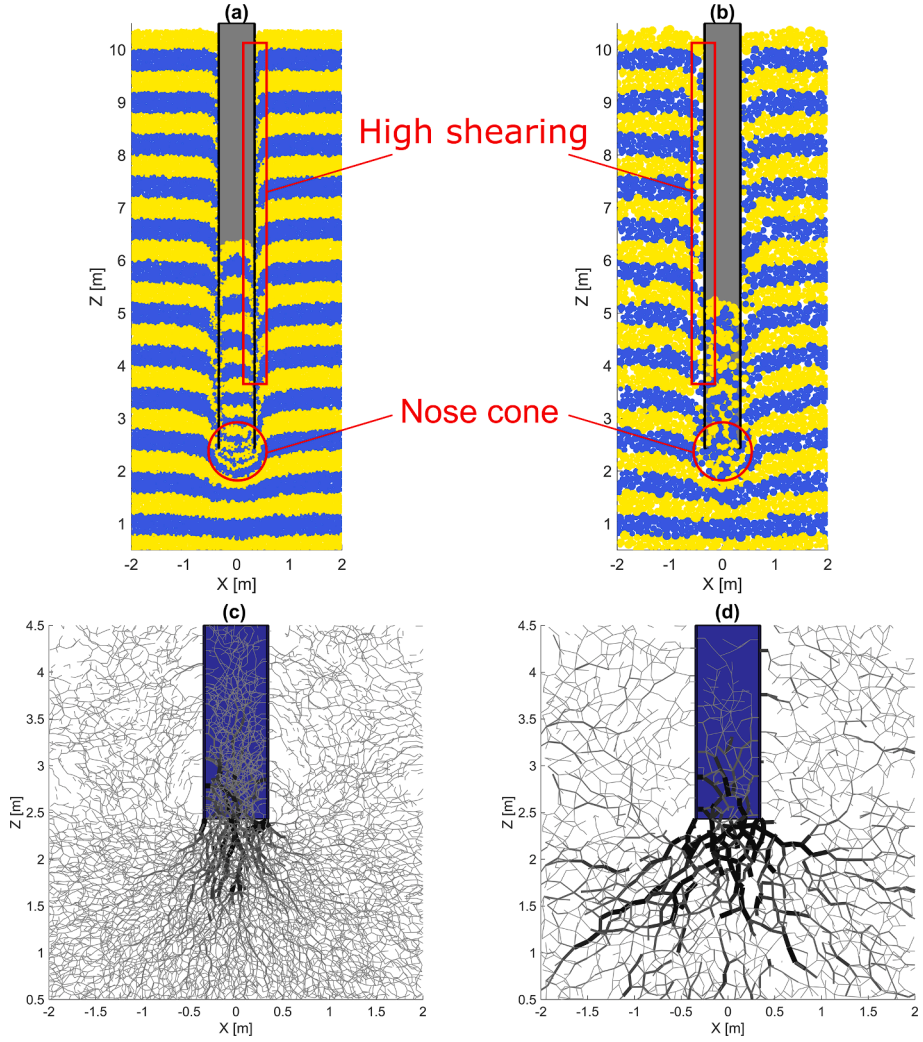

Fig. 5. Cross-section of particle positions at the end of plain jacking installation of pile P2 (a) for SF = 10 and (b) SF = 20. Force chains (forces greater than 2kN) around the pile tip for (c) SF = 10 and (d) SF = 20. Particles were coloured as a function of their initial position, in horizontal layers of 0.4 m. Line thickness is proportional to the contact force magnitude (max force equal to 100kN and 300kN respectively).

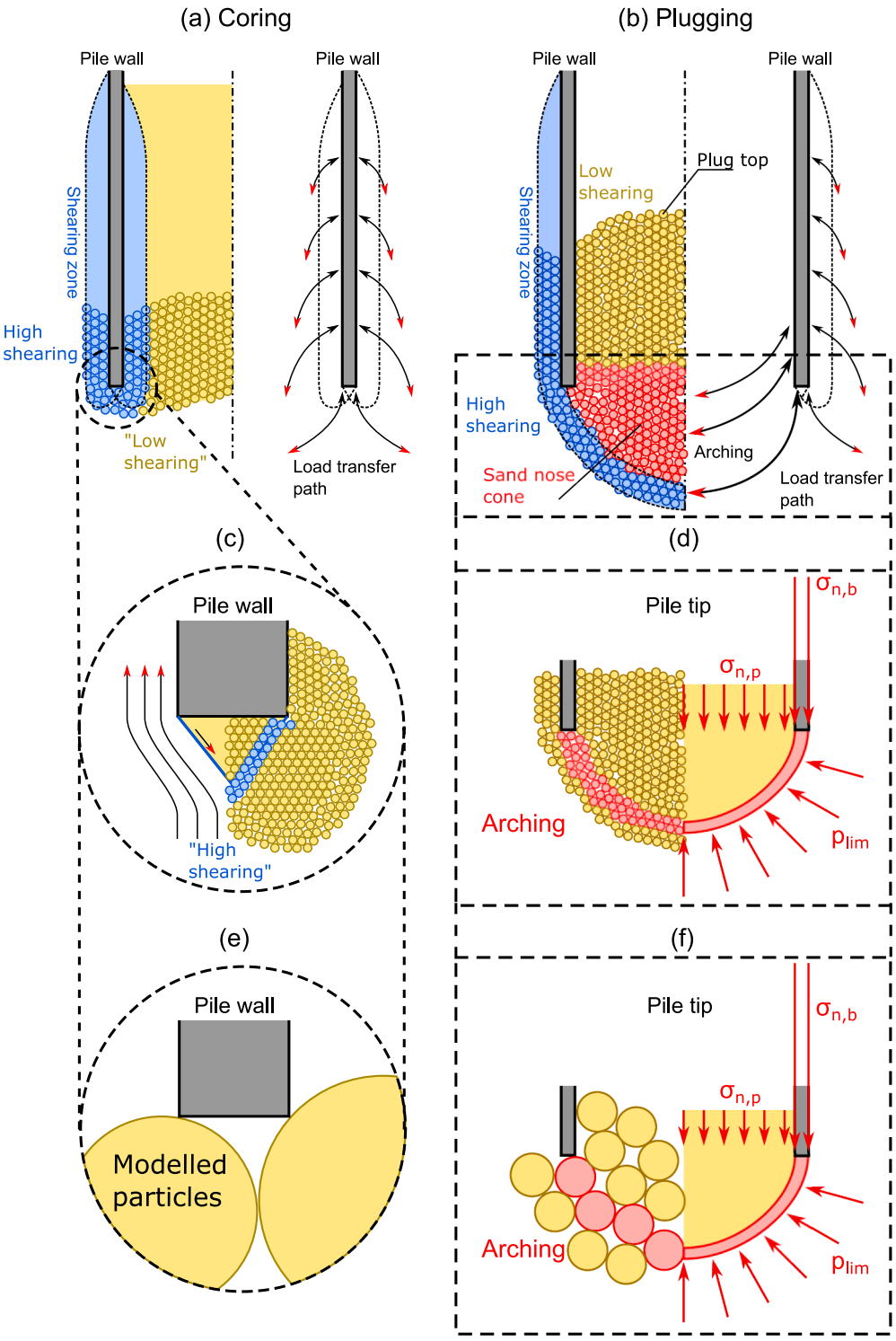

Fig. 6. Schematic description of the coring (a) and plugging (b) processes: particle displacement, shearing and load transfer. Effect of the particle scale effect (c,e) on the wall penetration resistance, (d,f) on pile plugging. Realistic particle to pile dimensions ratios are illustrated in (a-d), while the modelled particle to pile dimension ratios are illustrated in (e-f). The figure was inspired by Li et al. (2019, 2020) and adapted as a function of the results from this paper.

occur under such large forces/stresses, as shown by Yang et al. (2010) and Ciantia et al. (2019). One consequence of particle crushing is a reduction of the pile tip resistance with respect to a non-crushable material (Ciantia et al., 2019). A subsequent effect is the modification of the apparent friction coefficient at the pile wall, as particle breakage modifies the particle size distribution, hence the roughness to median particle dimension ratio (R_a/d_{50}), hence the friction coefficient (Ho et al., 2011). These phenomena were not modelled here.

The wall tip penetration mechanism generates high shearing and deflection of particles on each side of the wall (idealisation in Fig. 6c). The hypothesis of shear bands forming in a continuum soil is valid if particles are small enough (Fig. 6c), but a different more discrete mechanisms takes place if particles are larger (Fig. 6e), as is the case for both SF. Besides, smaller particles are less constrained than bigger ones and have more opportunities to reorganise to accommodate the penetrating pile. Therefore, a greater force is necessary to ensure pile

penetration in the largest SF granular bed and larger oscillations (smoothed in previous figures) of the measured force take place, as particles are suddenly displaced.

It was clear from results depicted in section 3.1 that the annular base attracted a higher force and stress than the plug. This could be idealised as shown in Fig. 6d. During the pile penetration, some arching takes place, supported by the pile annular tip. This arching shields the plug, which is subjected to a lower magnitude stress. Larger particles are more easily locked in a protective shield, hence the greater annular base stress and lower plug stress. Finally, Fig. 5b shows that the granular "nose cone" is less clearly defined for SF = 20, as the larger soil particle assembly is less easily deformed or increased in width. The shape of this nose cone is such that it is less effective at deflecting particles laterally, hence the greater force required in the plugging phase.

Both coring and plugging mechanisms are exposed to particle scaling issues. An adequate representation of the coring mechanism would require a high wall thickness to particle diameter ratio (t/d_{50}), which is smaller or equal to 0.28 in this work. The transition from coring to plugging is also dependent on the D/d_{50} ratio. Smaller particles (SF < 10) would be ideal to improve the accuracy of the coring mechanism modelling, but would prove computationally prohibitive.

3.2. Effect of SF on rotary jacking

3.2.1. Macroscopic observations

Rotary jacking induces an additional non-symmetrical shearing mechanism along the pile shaft and the base, which is known to reduce the pile penetration resistance (Deeks et al., 2010; Sharif et al., 2021d). The resulting failure mechanism in the ground, the consequences of the pile rotation on plugging and scaling effects will now be investigated for different imposed pile rotation rates. The change in failure mechanism also affects the observed particle scaling issues previously identified.

Pile P2 was rotary installed in the two granular beds (SF = 10 or 20) at two different installation pitches ($p_i = 1.73$ or 10) to uncover potential scaling issues. Overall, the total pile penetration resistance (Table 5) decreases with increasing installation pitch. Fig. 7a shows that the annular base stress strongly decreases with the installation pitch (-68% with respect to $p_i = 0$, for SF = 10) and exhibits the same SF dependence as plain jacking (-42% for SF = 10 with respect to SF = 20 at $p_i = 10$). The plug base stress is slightly reduced by the rotary installation (Fig. 7b). For SF = 10, the annular base to plug base stress ratio tends to 5, which is half the ratio measured for plain jacking. The outer shaft resistance is dramatically reduced with the pile rotation (Fig. 7c). Those reductions are consistent with previous experimental and numerical studies, which showed pitch-dependent reduction in the closed-ended pile base and shaft capacities with respect to plain jacking in sand (Deeks, 2008; Saathoff et al., 2020; Sharif et al., 2021c).

The change in shaft resistance is partly explained by the rotation of the maximum shear stress from the vertical direction to an inclined direction, due to the rotation of the pile (Deeks et al., 2010). However, the radial stress acting on the pile is also modified, as shown in Fig. 8. On the inside of the shaft (Fig. 8a), a rotating pile and smaller SF lead to greater radial stress. The plug length is also longer for a rotating pile, as shown in Fig. 7d, which is consistent with previous experimental results (Frick et al., 2018). Therefore, it can be concluded that rotary jacking and smaller particles favour a longer plug. The scaling effect is clear here as the maximum radial stress for SF = 10 is twice the one for SF = 20.

Finally, the radial stress decreases along the outer shaft with rotation of the pile (Fig. 8b). In this case, there is still some scaling effect (+100% difference from SF = 10 to 20). The reduction in radial stress is probably partly linked to plugging, as more coring means that a lower volume of material has to be pushed aside by the pile penetration. However, Sharif et al., (2021c) also observed the same reduction in radial stress for closed-ended piles, albeit of lower magnitude, suggesting there are some other mechanisms at play, probably inherent to the rotating nature of the shaft.

Table 5
Measured components of force at the end of the installation for plain and rotary jacking of pile P2.

p_i [-]	SF	F_{tot} [MN]	F_b [MN]	$F_{s,i}$ [MN]	$F_{s,o}$ [MN]
0	10	8.8	4.4	2.8	1.7
	20	12.0	7.8	1.6	2.6
	10 → 20	+36%	+79%	−42%	+52%
1.73	1.73	7.0	4.3	1.8	0.9
10	10	3.9	1.4	2.4	0.13
	20	3.8	2.2	1.4	0.17
	10 → 20	−3%	+57%	−42%	+30%

3.2.2. Microscopic observations

Microscopic observations again reveal the mechanisms during rotary jacking and enable interpretation of how particle scaling can affect the results. Fig. 9 shows particle displacement and force chains within the granular bed (SF = 10) after rotary jacking ($p_i = 10$). By comparison with plain jacking, the plug displays greater shearing (chevron shape) and there is a much smaller nose cone under the pile tip (Fig. 9a to be compared with Fig. 5a).

The plug also rotates with the pile at the end of installation (see Fig. 10b), which leads to more coring of the pile, with respect to the plain jacking case. This can be observed by plotting the relative vertical velocity, i.e. the particle velocity relative to the pile velocity. Comparison of Fig. 10c,d shows that the magnitude of the relative velocity inside the plug is larger for rotary jacking, indicating particles entering the pile. Consequently, as coring still dominates the installation, scaling effects were related to the non-dimensional ratio t/d_{50}, as detailed in Section 3.1.

Fig. 11 shows some plane cross-section of particle positions and force chains. The particles were coloured as a function of their initial position and Fig. 11(a-c) show that large magnitude in-plane shearing (due to pile rotation) took place in addition to the vertical shearing shown in the previous Fig. 9. Fig. 11d also shows that force chains are lower in amplitude inside a thin annular area around the pile shaft. This can be correlated to the lower radial stress depicted in Fig. 8 for rotary jacking. It can be assumed that force chains reorganise and create some form of in-plane arching around the pile shaft, to accommodate the continuous shearing and disturbance created by the rotary pile. Such a phenomenon will develop more easily in smaller particles (SF = 10) than in larger particles (SF = 20), which have more freedom to reorganise themselves.

Rotary jacking modifies the stress state under the base/plug, as shown in section 3.2.1. The contact force magnitude is reduced (Fig. 9b compared with Fig. 5b) and their orientation is modified, which is difficult to reproduce in a single 2D figure. Instead, the components of contact forces in local axisymmetric coordinates can be calculated, as described in Fig. 12. At each contact point between two particles, local radial (u_ρ), orthoradial (u_θ) and vertical (u_z) axes can be calculated, and the contact force can be decomposed along these vectors into (F_ρ, F_θ and F_z). These forces are plotted in Fig. 13 to show contact forces around the pile tip. Fig. 13a,c shows a rotation of the rotary jacking forces with respect to the plain ones, i.e. the ortho radial forces are greater in magnitude with respect to the vertical forces.

The difference between plain and rotary jacking mechanisms can be explained as follows. It can be postulated that the arching mechanism (nose cone, Fig. 6d,f) is a metastable structure. Plain jacking creates a generally symmetrical loading of this structure, which helps the nose cone to remain in place (Fig. 14a), even though plugging is known to evolve in an "on/off" manner (Randolph and Nicola, 1999). In contrast, the rotating pile creates some out of plane shearing along the base of the pile (τ_θ, Fig. 14b). This shearing is antisymmetric around the base and may destabilise the forming nose cone, breaking existing force chains. The forming nose cone would then collapse or would simply never form, reducing the normal force acting on the pile base and inducing more coring, as observed in the simulations. Such a mechanism is again

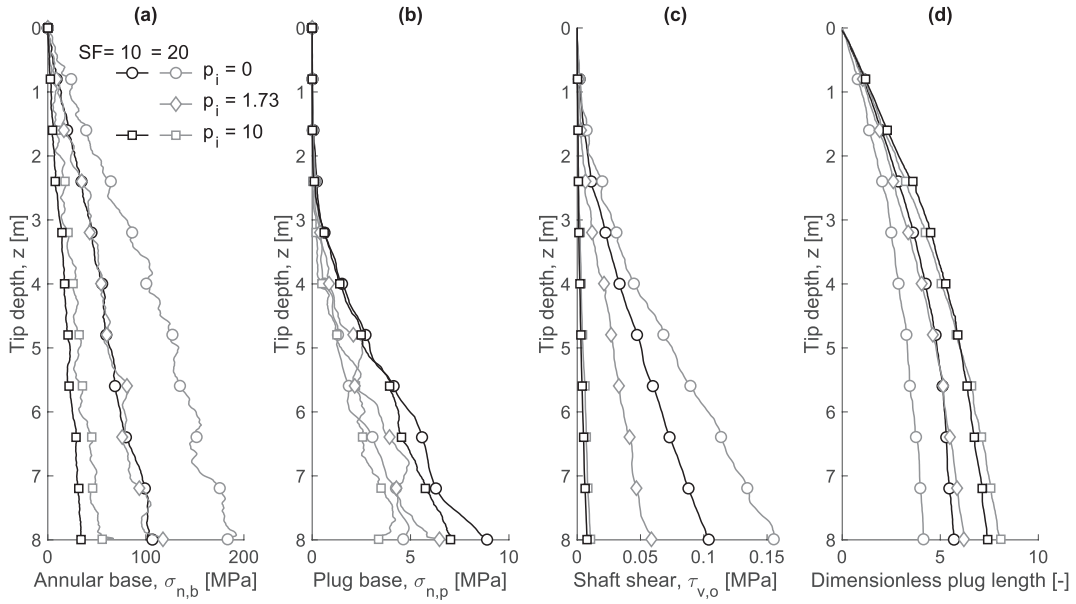

Fig. 7. Normalised results for rotary jacking: (a) Normal stress on the pile annular base ($\sigma_{n,b}$); (b) Normal stress on the plug base ($\sigma_{n,p}$); (c) Average shear stress on the external part of the shaft ($\tau_{v,o}$); (d) Dimensionless plug length (L_{plug}/D), during the jacking installation of pile P2 (D = 0.7 m) in two granular beds (SF = 10 or 20) at different installation pitches (p_i = 0, 1.73 or 10).

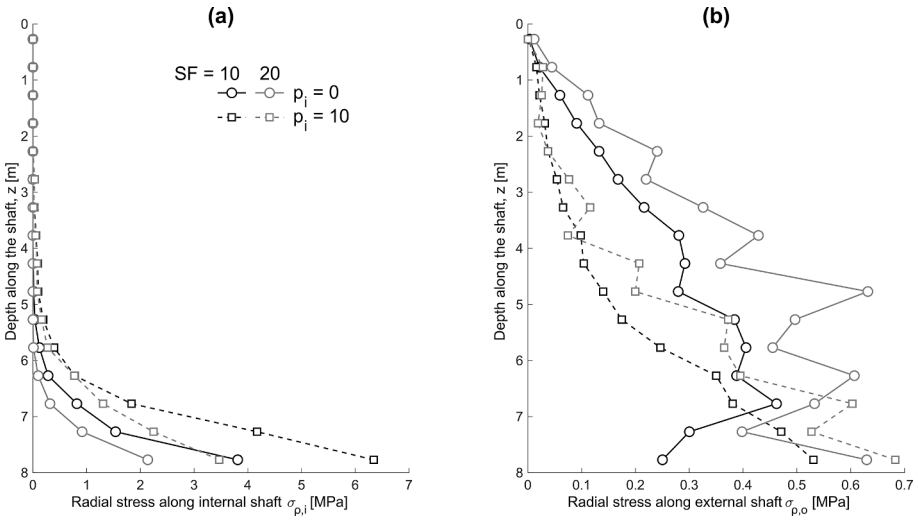

Fig. 8. Cross-section of the radial stress distribution at the end of installation, during the jacking installation of pile P2 (D = 0.7 m) in two granular beds (SF = 10 or 20) at different installation pitches (p_i = 0 or 10). (a) Inside the shaft, and (b) outside the shaft.

favoured by the use of smaller particles, which are less constrained in their displacements.

3.3. Potential boundary effects

The chamber to pile diameter ratios used in experimental studies is often in the range 15–42 with near-zero radial strain boundary conditions (Lehane and Gavin, 2001; Jardine et al., 2013b). In DEM studies, the same ratio is of the order of 15–28 (Arroyo et al., 2011; McDowell et al., 2012; Zhang et al., 2019; Khosravi et al., 2020) with constant radial stress boundary conditions. In both cases, researchers aim at minimising boundary effects and cost of experiments or simulations. However, Salgado et al. (1998) showed, using cavity expansion, that a very large (>100) chamber diameter to pile diameter ratio could be necessary to efficiently mimic field conditions during the penetration of a CPT cone. Jardine et al. (2013a) showed in highly instrumented calibration chamber tests that a significant change in the stress field could occur at a radial distance equal to 10 pile diameters, although the largest changes occur within 5 pile diameters. The lower chamber to pile diameter ratio adopted in this study (6–8.5) could lead to boundary effects, as the plastic zone could extend beyond the actual boundary.

A 2D axisymmetric finite element analysis (cylindrical cavity expansion) has been undertaken in the FE code PLAXIS (PLAXIS, 2017) to estimate the error on the pile penetration resistance. A 1 m high strip in vertical plane strain conditions was subjected to cavity expansion to a final radius of 0.35 m, which corresponds to pile P2 radius. In the reference case, the soil domain was modelled by the elastoplastic HSsmall model (Brinkgreve et al., 2000), with parameters corresponding to the HST95 sand at the same porosity as the DEM simulations (see Cerfontaine et al., 2019 for the parameters). Another truncated domain, was composed of a near-field domain (radius equal to 2.13 m, as per the DEM) whose behaviour was modelled by the HSsmall model, while the rest of the domain was assigned elastic properties, identical to the one assigned to the servo-control in the DEM simulation. The error in the

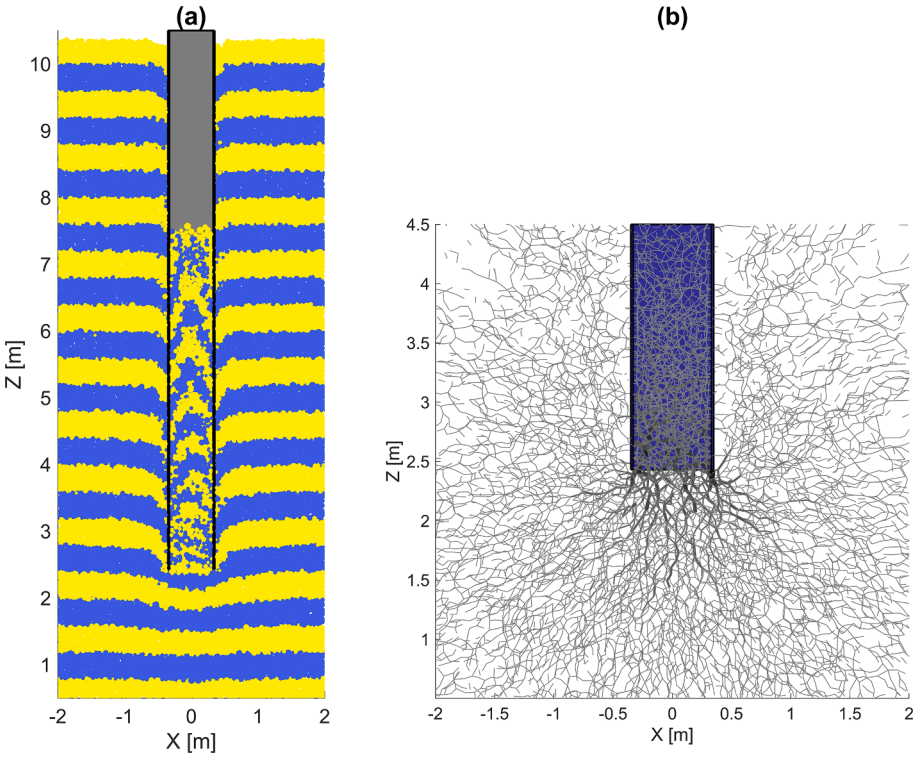

Fig. 9. (a) Cross-section of particle positions at the end of rotary ($p_i = 10$) jacking installation of pile P2 for SF = 10. (b) Force chains (forces greater than 2kN, capped at 200kN) around the pile tip. Particles were coloured as a function of their initial position, in horizontal layers of 0.4 m.

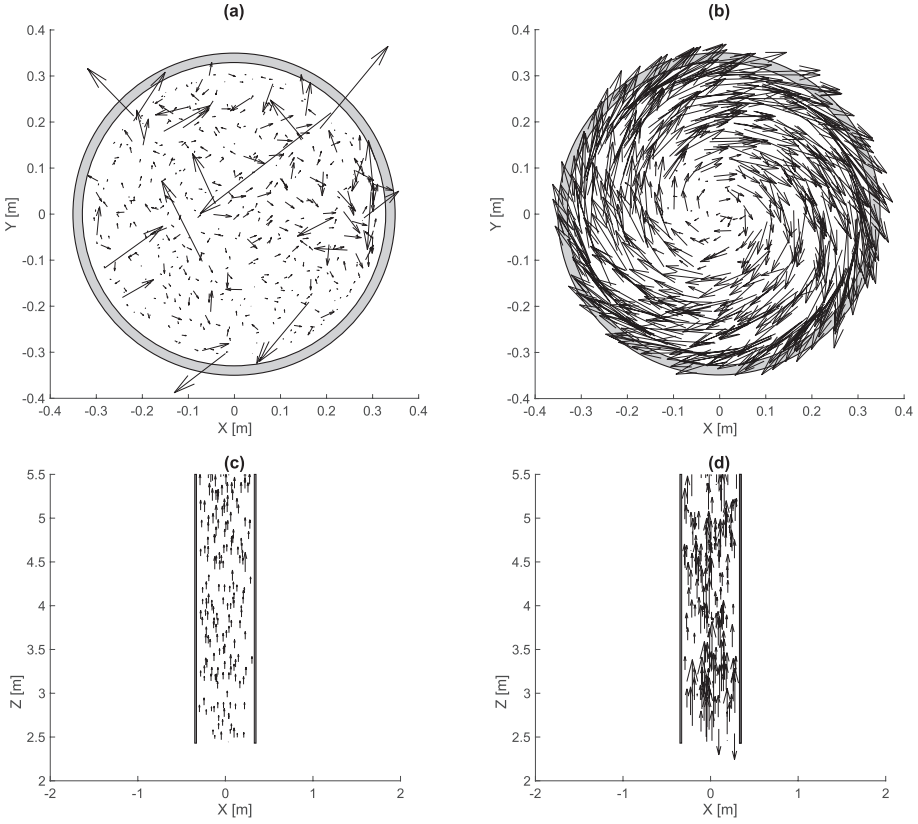

Fig. 10. Comparison of the X-Y plane component of the velocity field inside the plug at the tip depth (z = 8 m) for (a) plain jacking and (b) rotary jacking ($p_i = 10$). Comparison of X-Z plane component of the relative vertical velocity field (velocity of particle minus velocity of pile) for (c) plain jacking and (d) rotary jacking ($p_i = 10$). Scales are different in figure (a) and (b) for clarity. Scales are identical in figures (c) and (d) but only 1/10th of points are represented.

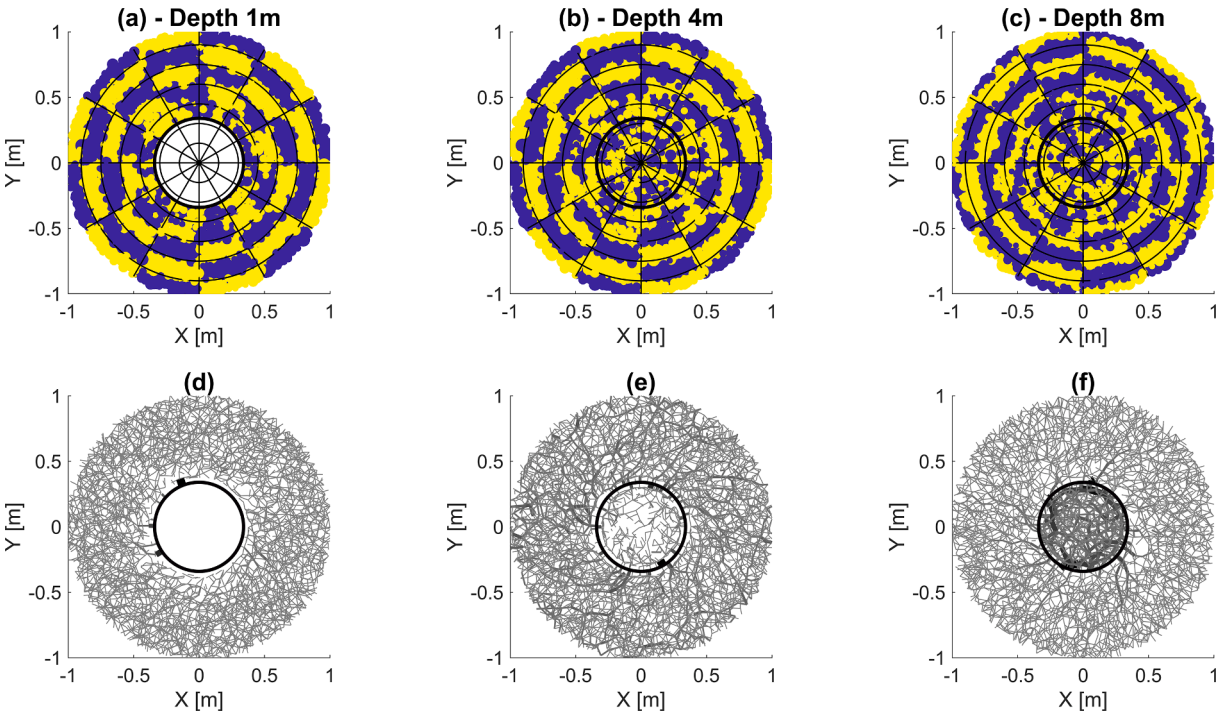

Fig. 11. Particle positions (a-c) and force chains (d-f) after rotary installation, pile P2, $p_i = 10$. Plane view at depth s equal to 1 m (a,d), 4 m (b,e) and 8 m (c,f), slice thickness equal to 0.3 m.

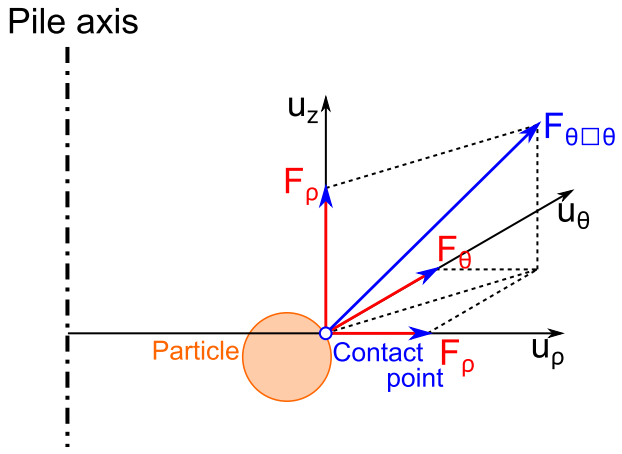

Fig. 12. Calculation of contact force components in local axes.

wall pressure magnitude calculated for the truncated domain could then be calculated by comparison with the non-truncated domain, at two different initial stress states corresponding to 2.25 m and 9.75 m depths.

In the granular bed with SF = 10, used as the reference, the maximum equivalent deviatoric strain induced by the pile P2 installation in the servo-controlled cylinders ranged from 0.45% (mid-depth = 2.25 m) to 1.6% (mid-depth = 9.75 m). Mapping those DEM maximum deviatoric strains to the finite element results, it is possible to estimate the error occurring in the estimation of the pile penetration resistance, due to the truncation of the domain. This error varies between −20% and 18% at 2.25 m depth and −16% and 47% at 9.75 m at the end of the final embedment depth. This error is an upper bound, for the largest embedment depth of the largest pile in SF = 10, which is considered the most realistic granular bed. Simulations with larger SF generally lead to a greater deviatoric strain, hence to a larger overestimation on the pile tip penetration resistance.

For the rotary jacking simulation, the deviatoric strain at the boundary was 2 or 3 times lower than for plain jacking, indicating a lower induced error caused by the boundary. In addition, the particles at the boundary did not show any significant circumferential displacement, which suggests that friction at the boundary was sufficient to mimic the retaining effect of the far field soil.

4. Limitations and recommendations

Three dimensional simulations are necessary to qualitatively and quantitatively reproduce pile plain and rotary jacking. Upscaling particles and using smaller granular domains coupled with servo-controlled boundaries can significantly reduce the computational cost of the modelling of boundary value problems. However, those simplifications can lead to an overestimation of the pile penetration resistance. Firstly, it can be concluded that a constant elastic stiffness servo-control should be improved to further minimise boundary effects, for instance by including an elastic perfectly plastic behaviour (Yu, 2000). Secondly, while particle upscaling was shown to have limited influence on the modelling of screw piles behaviour in sand (Cerfontaine et al., 2021b; Sharif et al., 2021c) or cone penetration (Ciantia et al., 2019), particle scaling issues could be identified for pile plain and rotary jacking of open ended piles where the additional length scale of the pile wall thickness is introduced. The effect of upscaling clearly depends on the physical mechanism at play during the pile installation.

Two mechanisms exist during the installation of plain and rotary jacked piles: coring and plugging. The prevalence of one or the other subsequently affects the stress field around the pile, hence its further resistance to axial loading. For instance, it was shown that the radial stress along the shaft, hence its resistance, is greater if larger particles are used, although this effect is also affected by the truncated domain adopted. The ratio t/d_{50} should be maximised to capture the coring mechanism, and the ratio D/d_{50} should be maximised to accurately capture the installation resistance of plugged pile. Both plain and rotary jacking installation are affected by scaling issues, but the coring mechanism is more prevalent in the latter, hence the importance of the ratio t/d_{50}.

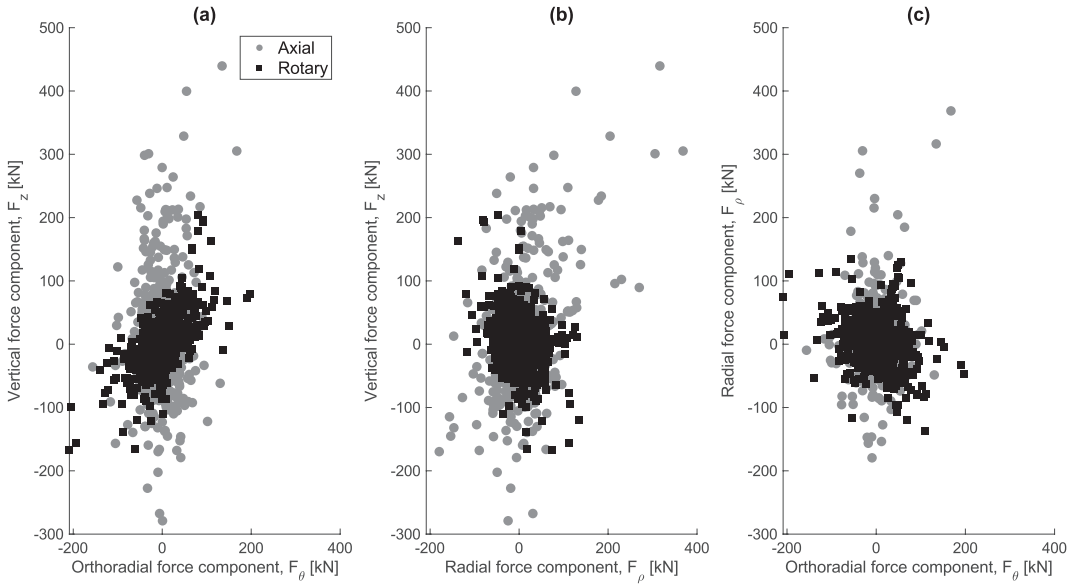

Fig. 13. Components of the contact forces in axisymmetric coordinates around the pile tip ($z_{tip} - 0.2$ m $\leq z \leq z_{tip} + 0.2$ m, $\rho \leq 0.6$ m), at the end of installation, SF = 10, for plain and rotary jacking. All normal contact forces are in compression.

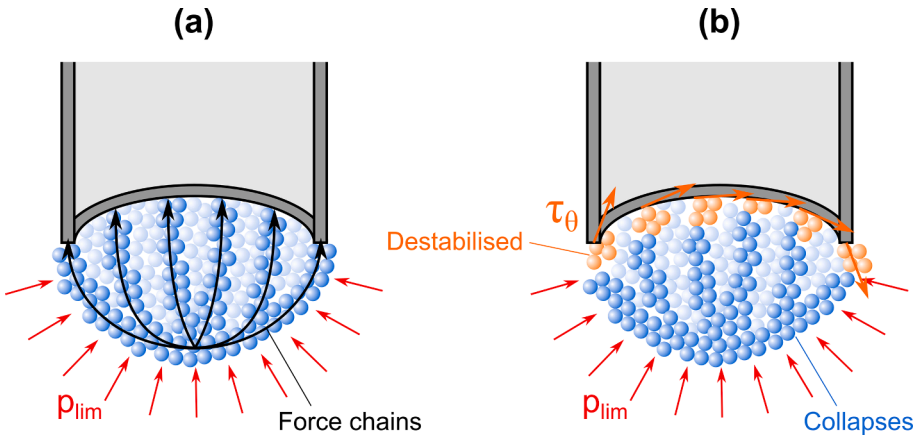

Fig. 14. Schematic of potential mechanisms for (a) plain and (b) rotary jacking.

Recommendations can be extended from the numerical to the physical modelling field of research, which both assume that granular beds behave like a continuum while modelling boundary value problems. On one hand, DEM simulations can be used to determine a conservative lower bound of relevant ratios (t/d_{50}, D/d_{50}) so that mechanisms are well captured in experiments. On the other hand, it should be noted that the size of particles at the smallest SF at prototype scale approaches the real size of cobble. Consequently, this shows that DEM simulation of boundary value problems can already approach the modelling of particles at their real size, albeit with a non-realistic shape. The results then suggest that the pile behaviour in sand and cobbles (different particle sizes) would be different, even if identical properties were measured for the behaviour of a representative elementary volume, e.g. triaxial test with enough particles.

A limitation of this work is the inability of particles to rotate (although this improves the match of the stress:strain response with soil element tests), while it has been recognised that shear planes induce particle rotation (Ma et al., 2018; Miyai et al., 2019; Zhu and Yin, 2019). A more extensive and cautious DEM calibration could be undertaken to determine rotational stiffness parameters associated with spherical particles or to use non-spherical particles (Rorato et al., 2021). The importance of shearing zones in the formation of the nose cone or around the rotating pile were identified in sections 3.1.2 and 3.2.1, and it could be assumed that the ability of particles to rotate would ease shear deformation.

Another limitation is the use non-crushable particles. The high vertical stress under the pile tip (>100 MPa at the end of installation) suggests that particle crushing will occur during pile penetration, consistently with previous experimental (White and Bolton, 2004) or numerical (Ciantia et al., 2019) studies. Consequently, the pile penetration resistance is probably overestimated with respect to reality, due to a reduced base penetration resistance, but also due to a reduction in shaft friction following a modification of the soil particle size distribution (Yang et al., 2010).

There is no magical solution to particle scaling issues. Results have shown that the different phenomena related to plain and rotary jacking can be qualitatively captured by a DEM model, and also how these phenomena are affected by scaling issues. However, quantitative prediction would require the simulation of several SF until it can be demonstrated that the scaling effect becomes negligible or that it does not affect the most relevant mechanism, e.g. plugged penetration at deep embedment depths. From a practical point of view, a good balance must be found between accuracy of the simulations and computational time.

5. Summary & Conclusions

Recent studies have shown that the DEM can be used to quantitatively reproduce small-scale centrifuge or calibration chamber experiments on the installation of piles in granular materials. This paper uses granular beds with the properties of the same sand material at the same target porosity, described with different particle scaling factors (SF). A constant stiffness boundary condition was applied to reduce the computational cost. This paper explores the influence of the SF on the measured pile penetration resistance and plugging behaviour during plain and rotary jacking of open-ended piles in 3D granular beds.

Results showed that the two granular beds behaved as different soils, ranging from sand to cobbles and coarse gravel, despite being assigned the properties of a sand. Reducing the SF significantly decreases the pile penetration resistance as larger particles are more easily locked in a nose cone at the tip of the pile. It was shown that the main particle scaling issues were related to the pile wall thickness to median particle size diameter ratio (t/d_{50}), which affects the coring mechanism and the transition to a fully plugged section. Earlier plugging and larger particles lead to more soil lateral displacement during the pile penetration and ultimately to greater radial stress along the outer shaft. This will ultimately affect the pile axial capacity. Consequently, the particle SF is important to make accurate predictions of pile installation and capacity, and the use of large particles can lead to shaft capacity overestimation.

The stress calculated under the annular pile base was shown to be 5 to 10 times higher than the stress acting at the base of the soil plug, even in almost fully plugged conditions. This observation partly results from scaling issues, as the base to plug stress ratio was decreased by reducing the SF.

Rotary jacking induces a rotation of the principal stresses under the pile tip and in the plug and a reduction in stress magnitude. The pile rotation creates some torsional shear stress under the tip that destabilises the nose cone and favours the coring mechanism. It was also shown that significant rotational shear was created around the pile shaft and inside the plug. Finally, it was shown that rotary and plain jacking were both affected in a similar way by the particle sizes.

Throughout the analysis of the results, this paper has highlighted limitations and potential for improvement of the simulations. For instance, particle breakage could be incorporated and the pile model could be represented with a geometrical roughness. The combination of those two modifications would automatically accounts for change in dilative and frictional behaviour of the shear zone adjacent to the pile shaft due to a change in particle size distribution. An enhancement of the contact model to include rotational stiffness would enable a better reproduction of physical mechanisms such as shear bands. Finally, the use of an elastoplastic servo controlled boundary conditions has a great potential to improve the accuracy of the simulations, while maintaining a low simulation time.

Despite those limitations, there is a clear trend that DEM will be more and more adopted to simulate boundary value problems to obtain useful insights into physical mechanisms at play. This paper showed that solutions exist to improve the computational efficiency of simulations and highlighted some ways of enhancing the accuracy of predictions. The continuous increase in computer capacity will make those solutions even more accessible in the future and will unlock the use of DEM for a wider range of users.

CRediT authorship contribution statement

Cerfontaine, B.: Conceptualization, Formal analysis, Writing - original draft, Visualization, Software. **Ciantia, M.:** Conceptualization, Resources, Software, Writing - review & editing. **Brown, M.J.:** Conceptualization, Writing - review & editing. **White, D.J.:** Writing - review & editing. **Sharif, Y.U.:** Software.

Declaration of Competing Interest

The authors declare that they have no known competing financial interests or personal relationships that could have appeared to influence the work reported in this paper.

Data availability

Data will be made available on request.

References

Al-Defae, A.H., Caucis, K., Knappett, J.A.A., 2013. Aftershocks and the whole-life seismic performance of granular slopes. Géotechnique 63 (14), 1230–1244. https://doi.org/10.1680/geot.12.P.149.

Arroyo, M., Butlanska, J., Gens, A., Calvetti, F., Jamiolkowski, M., 2011. Cone penetration tests in a virtual calibration chamber. Geotechnique 61 (6), 525–531. https://doi.org/10.1680/geot.9.P.067.

Bienen, B., Klinkvort, R.T., O'Loughlin, C.D., Zhu, F., Byrne, B.W., 2018. Suction caissons in dense sand, part I: Installation, limiting capacity and drainage. Géotechniqueotechnique 68 (11), 937–952. https://doi.org/10.1680/jgeot.16.P.281.

Bolton, M.D., Gui, M.W., Garnier, J., Corte, J.F., Bagge, G., Laue, J., Renzi, R., 1999. Centrifuge cone penetration tests in sand. Géotechnique 49 (4), 543–552. https://doi.org/10.1680/geot.1999.49.4.543.

Brinkgreve, R., Engin, E., Engin, H., 2000. Validation of empirical formulas to derive model parameters for sands. Numer. Methods Geotechn. Eng. 137–142. https://doi.org/10.1201/b10551-25.

Brown, M.J., Ishihara, Y., 2021. Predicting the capacity of push and rotate piles using offshore design techniques and CPT tests, Proceedings of the Second International Conference on Press-in Engineering 2021, Kochi, Japan, pp. 133–141. http://doi.org/10.1201/9781003215226-14.

Calvetti, F., 2008. Discrete modelling of granular materials and geotechnical problems, Revue européenne de génie civil, 12(7–8), pp. 951–965. http://doi.org/10.3166/ejece.12.951-965.

Cerfontaine, B., Knappett, J.A., Brown, M.J., Bradshaw, A.S., December 2018. (2019) Effect of soil deformability on the failure mechanism of shallow plate or screw anchors in sand. Comput. Geotech.. Elsevier 109, 34–45. https://doi.org/10.1016/j.compgeo.2019.01.007.

Cerfontaine, B., Brown, M. J., Ciantia, M. O., Huisman, M. and Ottolini, M., 2021a. Discrete element modelling of silent piling group installation for offshore wind turbine foundations., in Matsumoto, Ueno, Isobe, Nishioka, & W. (ed.) Proceedings of the Second International Conference on Press-in Engineering (ICPE2021). Koichi, Japan: Taylor & Francis Group, London, pp. 227–236.

Cerfontaine, B., Ciantia, M., Brown, M.J., Sharif, Y.U., 2021b. DEM study of particle scale and penetration rate on the installation mechanisms of screw piles in sand. Comput. Geotech.. Elsevier Ltd 139 (11), 104380. https://doi.org/10.1016/j.compgeo.2021.104380.

Ciantia, M.O., Arroyo, M., Butlanska, J., Gens, A., 2016. DEM modelling of cone penetration tests in a double-porosity crushable granular material. Comput. Geotechn. Elsevier Ltd 73, 109–127. https://doi.org/10.1016/j.compgeo.2015.12.001.

Ciantia, M.O., Boschi, K., Shire, T., Emam, S., 2018. Numerical techniques for fast generation of large discrete-element models. Proc. Inst. Civil Eng. – Eng. Comput. Mech. 171 (4), 147–161.

Ciantia, M.O., O'Sullivan, C., Jardine, R.J., 2019. Pile penetration in crushable soils : Insights from micromechanical modelling. In: Proceedings of the XVII ECSMGE-2019. Reykjavik, Iceland, Iceland, pp. 298–317. http://doi.org/10.32075/17ECSMGE-2019-1111.

Deeks, A.D., White, D.J., Ishihara, Y., 2010. Novel piling:Axial and rotary jacking, in Conference of the deep foundation institute. London, p. 24.

Deeks, A.D., 2008. An investigation into the strength and stiffness of jacked piles in sand. University of Cambridge, UK. Available at: http://publications.eng.cam.ac.uk/328467/.

Desrues, J., Viggiani, G., 2004. Strain localization in sand: An overview of the experimental results obtained in Grenoble using stereophotogrammetry. Int. J. Numer. Analyt. Methods Geomech., 28, 4, pp. 279–321. http://doi.org/10.1002/nag.338.

Duan, N., Cheng, Y.P., Lu, M., Wang, Z., 2021. DEM investigation of sand response during displacement pile installation. Ocean Eng.. Elsevier Ltd 230 (March), 109040. https://doi.org/10.1016/j.oceaneng.2021.109040.

Esposito, R.G., Velloso, R.Q., Jr, E. do A.V., Danziger, B.R., 2018. Multi-scale sensitivity analysis of pile installation using DEM, Computational Particle Mechanics. Springer International Publishing, 5, 3, pp. 375–386. http://doi.org/10.1007/s40571-017-0175-2.

Fan, S., Bienen, B., Randolph, M.F., 2019. Centrifuge study on effect of installation method on lateral response of monopiles in sand. International Journal of Physical Modelling in Geotechnics 1–13. https://doi.org/10.1680/jphmg.19.00013.

Frick, D., Schmoor, K. A., Gütz, P. and Achmus, M., 2018. Model testing of rotary jacked open ended tubular piles in saturated non-cohesive soil. In: Proceedings of Physical Modelling in Geotechnics, pp. 1347–1352. http://doi.org/10.1201/9780429438646-92.

Garnier, J., Gaudin, C., Springman, S. M., Culligan, P. J., Goodings, D., Konig, D., Kutter, B., Phillips, R., Randolph, M. F., Thorel, A., Garnier, J., Gaudin, C., Springman, S. M., Culligan, P. J., Goodings, D. et al., 2007. Catalogue of scaling laws and similitude questions in geotechnical centrifuge modelling, Int. J. Phys. Modell. Geotechn., 7, 3, pp. 01–23. http://doi.org/10.1680/ijpmg.2007.070301.

Han, F., Ganju, E., Prezzi, M., Salgado, R., Zaheer, M., 2020. Axial resistance of open-ended pipe pile driven in gravelly sand. Geotechnique 70 (2), 138–152. https://doi.org/10.1680/jgeot.18.P.117.

Henke, S., Bienen, B., 2014. Investigation of the influence of the installation method on the soil plugging behaviour of a tubular pile. Physical Modelling in Geotechnics -. In: Proceedings of the 8th International Conference on Physical Modelling in Geotechnics 2014. ICPMG 2014(2), 1995, pp. 681–687. https://doi.org/10.1201/b16200-94.

Ho, T.Y.K., Jardine, R.J., Anh-Minh, N., 2011. Large-displacement interface shear between steel and granular media. Geotechnique 61 (3), 221–234. https://doi.org/10.1680/geot.8.P.086.

Huang, X., Hanley, K.J., O'Sullivan, C., Kwok, C.Y., 2014. Exploring the influence of interparticule friction on critical state behaviour using DEM. Int. J. Numer. Anal. Meth. Geomech. 38, 1276–1297. https://doi.org/10.1002/nag.

Suits, L.D., Sheahan, T.C., Igoe, D., Doherty, P., Gavin, K., 2010. The Development and Testing of an Instrumented Open-Ended Model Pile. Geotech. Test. J. 33 (1), 102708.

Igoe, D.J.P., Gavin, K.G., O'Kelly, B.C., 2011. Shaft Capacity of Open-Ended Piles in Sand. J. Geotech. Geoenviron. Eng. 137 (10), 903–913. https://doi.org/10.1061/(asce)gt.1943-5606.0000511.

Ishihara, Y., Haigh, S., Koseki, J., 2020. Assessment of base capacity of open-ended tubular piles installed by the Rotary Cutting Press-in method. Soils Found Japan. Geotechn. Soc. 60 (5), 1189–1201. https://doi.org/10.1016/j.sandf.2020.07.006.

Itasca Consulting Group (2019) PFC3D 6.17.

Jardine, R., Chow, F., Overy, R., Standing, J., 2005. ICP design methods for driven piles in sands and clays. Thomas Telford Publishing. https://doi.org/10.1680/idmfdpisac.32729.

Jardine, R.J., Zhu, B.T., Foray, P., Yang, Z.X., 2013a. Interpretation of stress measurements made around closed-ended displacement piles in sand. Geotechnique 63 (8), 613–627. https://doi.org/10.1680/geot.9.P.138.

Jardine, R.J., Zhu, B.T., Foray, P., Yang, Z.X., 2013b. Measurement of stresses around closed-ended displacement piles in sand. Geotechnique 63 (1), 1–17. https://doi.org/10.1680/geot.9.P.137.

Jeanjean, P., Millar, D., Brooks, H. and Yogendrakumar, M., 2015. Lessons learned from pile driving and monitoring in gravels on the Northstar Artificial Island. In: Meyer, V. (ed.) Proceedings of Frontiers in Offshore Geotechnics III. Oslo, Norway: Taylor & Francis Group, London, pp. 587–593.

Khosravi, A., Martinez, A., DeJong, J., 2020. DEM simulations of CPT measurements and soil classification. Can. Geotech. J. 57 (9) https://doi.org/10.1139/cgj-2019-0512.

Khoubani, A., Evans, T.M., 2018. An efficient flexible membrane boundary condition for DEM simulation of axisymmetric element tests. Int. J. Numer. Anal. Meth. Geomech. 42 (4), 694–715. https://doi.org/10.1002/nag.2762.

Lauder, K.D., Brown, M.J., Bransby, M.F., Boyes, S., 2013. The influence of incorporating a forecutter on the performance of offshore pipeline ploughs. Appl. Ocean Res. Elsevier Ltd 39, 121–130. https://doi.org/10.1016/j.apor.2012.11.001.

Lauder, K., 2010. The performance of pipeline ploughs. University of Dundee, UK. PhD thesis.

Lehane, B., Gavin, K., 2001. Base resistance of jacked pipe piles in sand. J. Geotech. Geoenviron. Eng. 127 (6), 473–480.

Lehane, B.M., Schneider, J.A., Xu, X., 2007. Development of the UWA-05 design method for open and closed ended driven piles in siliceous sand. Geotechn. Spec. Publ. 40902 (158), 1–10. https://doi.org/10.1061/40902(221)12.

Li, L., Wu, W., Hesham El Naggar, M., Mei, G., Liang, R., 2019. DEM analysis of the sand plug behavior during the installation process of open-ended pile. Comput. Geotech.. Elsevier 109 (January), 23–33. https://doi.org/10.1016/j.compgeo.2019.01.014.

Li, L., Wu, W., Liu, H., Lehane, B., 2021. DEM analysis of the plugging effect of open-ended pile during the installation process. Ocean Eng. 220, 108375.

Li, L., Wu, W., Liu, H., Lehane, B., July 2020. (2021) DEM analysis of the plugging effect of open-ended pile during the installation process. Ocean Eng.. Elsevier Ltd 220, 108375. https://doi.org/10.1016/j.oceaneng.2020.108375.

Liu, J., Duan, N., Cui, L., Zhu, N., 2019. DEM investigation of installation responses of jacked open-ended piles, *Acta Geotechnica*. Springer, Berlin Heidelberg 14 (6), 1805–1819. https://doi.org/10.1007/s11440-019-00817-7.

Lobo-Guerrero, S., Vallejo, L.E., 2007. Influence of pile shape and pile interaction on the crushable behavior of granular materials around driven piles: DEM analyses. Granul. Matter 9 (3–4), 241–250. https://doi.org/10.1007/s10035-007-0037-3.

Lommen, S., Mohajeri, M., Lodewijks, G., Schott, D., 2019. DEM particle upscaling for large-scale bulk handling equipment and material interaction. Powder Technol. The Authors 352, 273–282. https://doi.org/10.1016/j.powtec.2019.04.034.

Ma, G., Regueiro, R.A., Zhou, W., Wang, Q., Liu, J., 2018. Role of particle crushing on particle kinematics and shear banding in granular materials. Acta Geotechnica Springer, Berlin Heidelberg 13 (3), 601–618. https://doi.org/10.1007/s11440-017-0621-6.

Martinez, A., Frost, J.D., 2017. Particle-scale effects on global axial and torsional interface shear behavior. Int. J. Numer. Anal. Meth. Geomech. 41 (3), 400–421. https://doi.org/10.1002/nag.2564.

McDowell, G.R., Falagush, O., Yu, H.S., 2012. A particle refinement method for simulating DEM of cone penetration testing in granular materials, Geotechn. Lett., 2 (7–9), pp. 141–147. http://doi.org/10.1680/geolett.12.00036.

Miyai, S., Kobayakawa, M., Tsuji, T., Tanaka, T., 2019. Influence of particle size on vertical plate penetration into dense cohesionless granular materials (large-scale DEM simulation using real particle size). Granular Matter Springer, Berlin Heidelberg 21 (4), 1–21. https://doi.org/10.1007/s10035-019-0961-z.

Paikowsky, S.G., Whitman, R.V., 1990. The effects of plugging on pile performance and design. Can. Geotech. J. 27 (4), 429–440. https://doi.org/10.1139/t90-059.

Plaxis, 2017. PLAXIS 2D Reference Manual. Delft, The Netherlands.

Randolph, M.F., Nicola, a. De 1999. Centrifuge modelling of pipe piles in sand under axial loads. Géotechnique, 49(3), pp. 295–318. http://doi.org/10.1680/geot.1999.49.3.295.

Rorato, R., Arroyo, M., Gens, A., Andò, E., Viggiani, G., 2021. Image-based calibration of rolling resistance in discrete element models of sand. Computers and Geotechnics 131 (December 2019). https://doi.org/10.1016/j.compgeo.2020.103929.

Rorato, R., Arroyo, M., Gens, A., Andò, E., Viggiani, G., December 2019. (2021) Image-based calibration of rolling resistance in discrete element models of sand. Comput. Geotech. 131 https://doi.org/10.1016/j.compgeo.2020.103929.

Saathoff, J.E., Frick, D., Achmus, M., 2020. Investigation of the behaviour of jacked and rotary-jacked piles in sandy soils, in Piling 2020: Proceedings of the Piling 2020 Confeference, pp. 241–246.

Sharif, Y.U., Brown, M.J., Ciantia, M.O., Knappett, J.A., Davidson, C., Cerfontaine, B., Robinson, S., B., C., Robinson, S. and Ball, J., 2019. Numerically modelling the installation and loading of screw piles using DEM, in Proceedings of the 1st International Symposium on Screw Piles for Energy Applications. Dundee, UK: University of Dundee, pp. 101–108.

Sharif, Y.U., Brown, M.J., Ciantia, M.O., Cerfontaine, B., Davidson, C., Knappett, J.A., Ball, J.D., 2021a. Assessing single-helix screw pile geometry on offshore installation and axial capacity. Proc. Inst. Civil Eng. – Geotechn. Eng. 174 (5), 512–529.

Sharif, Y.U., Brown, M.J., Cerfontaine, B., Davidson, C., Ciantia, M., Knappett, J., Brennan, A., Ball, J.D., Augarde, C., Coombs, W., Blake, A., Richards, D., White, D., Huisman, M., Ottolini, M., 2021b. Effects of screw pile installation on installation requirements and in-service performance using the Discrete Element Method. Can. Geotech. J. 58 (9), 1334–1350. https://doi.org/10.1139/cgj-2020-0241.

Sharif, Y.U., Brown, M.J., Ciantia, M.O., Cerfontaine, B., Davidson, C., Knappett, J., Meijer, G.J., Ball, J., 2021c. Using DEM to assess the influence of single helix screw pile geometry on the installation requirements and in-service axial capacity in dense sand. Can. Geotech. J. 58 (7), 919–935. https://doi.org/10.1139/cgj-2020-0017.

Sharif, Y.U., Brown, M.J., Ciantia, M.O., Cerfontaine, B., Davidson, C., Knappett, J., Meijer, G.J., Ball, J., 2021d. Using discrete element method (Dem) to create a cone penetration test (cpt)-based method to estimate the installation requirements of rotary-installed piles in sand. Can. Geotech. J. 58 (7), 919–935. https://doi.org/10.1139/cgj-2020-0017.

Shire, T., Hanley, K.J., Stratford, K., 2021. DEM simulations of polydisperse media: efficient contact detection applied to investigate the quasi-static limit. Comp. Part. Mech. 8 (4), 653–663.

Ting, J.M., Corkum, B.T., Kauffman, C.R., Greco, C., 1989. Discrete numerical model for soil mechanics. J. Geotech. Eng. 115 (3), 379–398.

White, D.J., Bolton, M.D., 2004. Displacement and strain paths during plane-strain model pile installation in sand. Geotechnique 54 (6), 375–397. https://doi.org/10.1680/geot.2004.54.6.375.

White, D.J., Schneider, J.A., Lehane, B.M., 2005. The influence of effective area ratio on shaft friction of displacement piles in sand. Front. Offshore Geotechn., ISFOG 2005, 741–748.

Wu, H., Gu, X., Hu, J., Zhou, Q., 2022. DEM simulation of small strain and large strain behaviors of granular soils with a coherent contact model. Granular Matter Springer, Berlin Heidelberg 24 (4), 1–15. https://doi.org/10.1007/s10035-022-01286-8.

Yang, Z.X., Jardine, R.J., Zhu, B.T., Foray, P., Tsuha, C.H.C., 2010. Sand grain crushing and interface shearing during displacement pile installation in sand. Geotechnique 60 (6), 469–482. https://doi.org/10.1680/geot.2010.60.6.469.

Yu, H.-S., 2000. Cavity Expansion Methods in Geomechanics. 1st edn. Springer Dordrecht. http://doi.org/10.1017/CBO9781107415324.004.

Zhang, X., Fatahi, B., 2021. Assessing axial load transfer mechanism of open-ended tubular piles penetrating in weak rocks using three-dimensional discrete element method, Computers and Geotechnics. Elsevier Ltd, 137(May), p. 104267. http://doi.org/10.1016/j.compgeo.2021.104267.

Zhang, Z., Wang, Y.H., 2015. Three-dimensional DEM simulations of monotonic jacking in sand. Granular Matter Springer, Berlin Heidelberg 17 (3), 359–376. https://doi.org/10.1007/s10035-015-0562-4.

Zhang, N., Arroyo, M., Ciantia, M. O., Gens, A. and Butlanska, J., 2019. Standard penetration testing in a virtual calibration chamber, Computers and Geotechnics. Elsevier, 111(February), pp. 277–289. http://doi.org/10.1016/j.compgeo.2019.03.021.

Zhu, H.-X., Yin, Z.-Y., 2019. Grain Rotation-Based Analysis Method for Shear Band. J. Eng. Mech. 145 (10), 04019073. https://doi.org/10.1061/(asce)em.1943-7889.0001654.